AFRL-AFOSR-VA-TR-2023-0112

Towards the understanding of the deformation mechanisms of refractory complex concentrated alloys exhibiting B2-type order

Michael Mills
OHIO STATE UNIVERSITY
1960 KENNY RD
COUMBUS, OH,
US

10/27/2022
Final Technical Report

Air Force Research Laboratory
Air Force Office of Scientific Research
Arlington, Virginia 22203
Air Force Materiel Command

REPORT DOCUMENTATION PAGE

PLEASE DO NOT RETURN YOUR FORM TO THE ABOVE ORGANIZATION.

1. REPORT DATE	2. REPORT TYPE	3. DATES COVERED	
20221027	Final	START DATE 20200930	END DATE 20210929

4. TITLE AND SUBTITLE
Towards the understanding of the deformation mechanisms of refractory complex concentrated alloys exhibiting B2-type order

5a. CONTRACT NUMBER	5b. GRANT NUMBER	5c. PROGRAM ELEMENT NUMBER
	FA9550-20-1-0231	61102F
5d. PROJECT NUMBER	**5e. TASK NUMBER**	**5f. WORK UNIT NUMBER**

6. AUTHOR(S)
Michael Mills

7. PERFORMING ORGANIZATION NAME(S) AND ADDRESS(ES)
OHIO STATE UNIVERSITY
1960 KENNY RD
COUMBUS, OH
US

8. PERFORMING ORGANIZATION REPORT NUMBER

9. SPONSORING/MONITORING AGENCY NAME(S) AND ADDRESS(ES)	10. SPONSOR/MONITOR'S ACRONYM(S)	11. SPONSOR/MONITOR'S REPORT NUMBER(S)
Air Force Office of Scientific Research 875 N. Randolph St. Room 3112 Arlington, VA 22203	AFRL/AFOSR RTA1	AFRL-AFOSR-VA-TR-2023-0112

12. DISTRIBUTION/AVAILABILITY STATEMENT
A Distribution Unlimited: PB Public Release

13. SUPPLEMENTARY NOTES

14. ABSTRACT
During the period from September 2020 to September 2021, we have investigated and reported the analysis of the deformation mechanisms at 600°C in a two-phase, BCC+B2, refractory complex concentrated alloy (RCCA) Al0.5NbTa0.8Ti1.5V0.2Zr. After annealing at 1200°C during 2h and subsequent water quenching, the alloy microstructure is unstable and dynamic coarsening of B2 precipitates is evidenced during the mechanical testing at 600°C. After true plastic strain of 0.030 at strain rate of 10â^'4 sâ^'1, the deformation becomes highly localized in wavy bands reflecting the profusion of cross-slip. Scanning transmission electron microscopy (STEM) observations highlight the presence of paired a/2<111> dislocations that shear the B2 precipitates in a cooperative process. In addition, some chemical segregation effect is observed along the narrow dislocation bands likely induced to decrease the antiphase boundary (APB) energy of the system. The analysis of the microstructure formed after an annealing at 600°C during 120h shows that the presence of discrete intermetallic particles in a disordered BCC matrix. These precipitates consist of semi-coherent B2 phase and also related ordered omega ones. After compressive testing at 600°C, the STEM observations reveal that plasticity occur by dislocation glide in the confined regions of the BCC matrix. No shearing events of the precipitates (B2 or omega phases) have been evidenced during the deformation

15. SUBJECT TERMS

16. SECURITY CLASSIFICATION OF:			17. LIMITATION OF ABSTRACT	18. NUMBER OF PAGES
a. REPORT U	b. ABSTRACT U	c. THIS PAGE U	UU	22

19a. NAME OF RESPONSIBLE PERSON	19b. PHONE NUMBER *(Include area code)*
MATTHEW KRISAK	

AFOSR AWARD FA9550-20-1-0231

Towards the understanding of the deformation mechanisms of refractory complex concentrated alloys exhibiting B2-type order

PO: Martin SCHMIDT
PI: Michael MILLS, Pr., The Ohio State University, Department of Materials Science and Engineering
Co-PI: Jean-Philippe COUZINIE, Pr., The Ohio State University, Department of Materials Science and Engineering

Technical Report - Summary

Award Number
FA9550-20-1-0231

Report type
Final Performance

Reporting periods
30 SEP 20 - 29 SEP 21

Distribution Statement
Distribution A - Approved For Public Release

Program Officer Name
Martin SCHMIDT

Principal Investigator Name
Michael MILLS

Project Title
Towards the understanding of the deformation mechanisms of refractory complex concentrated alloys exhibiting B2-type order

Abstract
During the period from September 2020 to September 2021, we have investigated and reported the analysis of the deformation mechanisms at 600°C in a two-phase, BCC+B2, refractory complex concentrated alloy (RCCA) $Al_{0.5}NbTa_{0.8}Ti_{1.5}V_{0.2}Zr$. After annealing at 1200°C during 2h and subsequent water quenching, the alloy microstructure is unstable and dynamic coarsening of B2 precipitates is evidenced during the mechanical testing at 600°C. After true plastic strain of 0.030 at strain rate of 10^{-4} s^{-1}, the deformation becomes highly localized in wavy bands reflecting the profusion of cross-slip. Scanning transmission electron microscopy (STEM) observations highlight the presence of paired a/2<111> dislocations that shear the B2 precipitates in a cooperative process. In addition, some chemical segregation effect is observed along the narrow dislocation bands likely induced to decrease the antiphase boundary (APB) energy of the system. The analysis of the microstructure formed after an annealing at 600°C during 120h shows that the presence of discrete intermetallic particles in a disordered BCC matrix. These precipitates consist of semi-coherent B2 phase and also related ordered omega ones. After compressive testing at 600°C, the STEM observations reveal that plasticity occur by dislocation glide in the confined regions of the BCC matrix. No shearing events of the precipitates (B2 or omega phases) have been evidenced during the deformation at 600°C.

Accomplishments

- **Background & Problem Statement**

For two decades, the concept of alloy design based on a multi-metallic "cocktail" associated with the high configurational entropy approach has opened up a new challenge in the materials science and engineering field. It has led to the design of high-entropy alloys (HEAs) which could be well suited for low and elevated temperature applications. HEAs are a promising route toward the development of innovative metallurgical systems, especially in the framework of structural applications. Among the most interesting HEAs, those made of refractory metals (Refractory High Entropy Alloys (RHEAs) or Refractory Complex Concentrated Alloys (RCCAs)) are promising and were originally developed for potential high temperature structural applications (blades, disks in aerospace industry, gas turbine engines, as examples; T_{use} > 1000°C) and they are currently viewed as new materials systems that may be able to compete with current nickel-based superalloys [1,2]. The most promising compositions are found in the Al-Mo-Nb-Ta-Ti-(V)-Zr system in which alloy matrix are either ordered B2 single phase or made of a fine (spherical or cuboidal) nano-coherent BCC precipitation in a B2 matrix. Alloys with such a microstructure are referred as refractory high-entropy superalloys, as they are inspired from the duplex γ/γ' microstructure of Ni-based superalloys which constitute a key factor for their mechanical performance. Some major basic and technical challenges have to be addressed to ensure that RCCAs have the opportunity to compete with superalloys for future structural applications. Among the main challenging points, the description of the deformation modes in RHEAs and RCCAs depicting B2 order is necessary to understand the mechanical behavior of these alloys systems. **The detailed description of these modes will also give crucial information's to improve the modeling and design of future potential interesting systems. Such analysis and understanding of the deformation processes was at the heart of the project.**

- **Research Objectives**

The current project aimed at describing and understanding the relationships between mechanical properties and underlying deformation processes of promising RCCAs exhibiting B2-type order. The ordered B2 phase is an important potential constituent in RCCAs and it is of utmost importance to examine the mechanical behavior of this phase. In such framework the current project was focusing on the analysis (mainly using STEM) of a BCC+B2 microstructure in the Al-Nb-Ta-Ti-V-Zr system deformed by compression at high temperature (600°C). Two microstructures were investigated: a co-continuous microstructure of BCC phase with the presence of B2 nano-clusters and one consisting of discrete B2 precipitates in a BCC matrix. The following points were mainly addressed and discussed:

- What are the nature and characteristics of the defects involved in the deformation of the RCCA exhibiting B2-order?
- What is the influence of the B2-order on the deformation mechanisms?

For this purpose, **the studied composition was $Al_{0.5}NbTa_{0.8}Ti_{1.5}V_{0.2}Zr$ ($Al_{10}Nb_{20}Ta_{16}Ti_{30}V_4Zr_{20}$, at.%)**. It has a relatively low density (7.4 g/cm^3) and displays high compressive strength that can exceed 2 GPa at RT and more than 1.7 GPa at 600°C after hot isostatic pressing (HIP) followed by a 1200°C / 24 h heat treatment [3]. It should be mentioned that mechanical properties can be tuned by heat treatments. An interesting compromise between yield strength (>1.4 GPa) and compressive ductility (close to 20 %) during mechanical testing at 600°C could be reached thanks to a long annealing leading to the formation of discrete B2 precipitates in a BCC matrix [4,5].

The investigation of the deformation processes has required 3 main tasks:

- Alloy preparation;
- Mechanical testing at 600°C;
- Microstructure characterization using cutting edge SEM and (S)TEM facilities of CEMAS at OSU.

The **alloy preparation** has been performed under vacuum arc melting in a water-cooled copper hearth from a mixture of respective metals with purity exceeding 99.9%. After solidification, the produced alloy button was wrapped in a Ta foil, hot isostatic pressed (HIPed) at 1200°C under a hydrostatic pressure of 207 MPa for 2 hours and then annealed for 24 hours at 1200°C. HIP and annealing were conducted in the atmosphere of high-purity argon, and heating and cooling rates were 15°C/min for HIP process and 20°C/min for the annealing process. The samples were additionally annealed at 1200°C for 2 h in a sealed quartz tube under argon atmosphere, and water quenched (WQ) (condition 2). From the latter heat treatment, some samples were also annealed at 600°C during 120h in sealed ampoules under inert atmosphere and WQ (condition 3).

Mechanical tests were performed at 600°C on rectangular-prism-shaped specimens with dimensions 4.05 mm x 4.05 mm x 7.05 mm extracted from the samples. The compression tests were conducted in a dynamic vacuum of 1×10^{-5} torr or better. The testing procedure consisted of (i) 50°C/min heating to 600°C, (ii) holding at the temperature for 15 min, (iii) compression deformation at a constant ram speed that provided an initial strain rate of 10^{-4} s^{-1} to an assigned strain and (iv) furnace cooling at zero power supply. During heating and soaking steps, the sample was under 20 N force control to protect from deformation due to dies expansion.

After testing, samples were cut along the compressive axis, mounted, ground using SiC papers and finally polished using active oxide polishing suspension (OPS) consisting of 50 nm colloidal silica. **Microstructures (conditions 2 and 3) were analyzed using scanning electron**

microscopy (SEM). SEM Apreo (Thermo Fisher Scientific, TFS) equipped with back-scattered electron (BSE) and electron back-scatter diffraction (EBSD) detectors was used to give insight into the deformation of the microstructure and the presence of slip traces on grain cross-sections. To do so, electron channeling contrast imaging (ECCI) was performed using 30 kV at low working distances. EBSD mappings of grain orientations were then collected in areas exhibiting slip traces and further analyzed using OIM TSL software in order to identify the crystallography of the involved active systems (slip direction and plane, and associated Schmid factors). TFS/FEI Helios dual-beam system equipped with focused ion beam (FIB) was used to extract TEM thin foils (lamellae) parallel or perpendicular to slip bands in selected grains to analyze dislocation patterning. **The lamellae parallel to <001> directions were also prepared to detail the atomic structure of the phases, before and after HT deformation**. **These foils were subsequently investigated in STEM mode using image-corrected and monochromated TFS/FEI Titan^3 G2 operating at 300 keV and S-CORR probe corrected and monochromated TFS Themis-Z at an acceleration voltage of 200 kV**. Dislocation analyses were performed on TFS/FEI Titan^3 G2, and STEM diffraction contrast imaging (STEM-DCI) was done with bright-field (BF) detector by selecting the appropriate camera length (CL). Determination of Burgers vectors was made using conventional **g**.**b** analysis, and slip planes were determined by trace analysis using stereographic projection and the pycotem toolbox developed by Mompiou and Xie. The TEM thin foils were tilted into specific low index crystallographic zones to perform atomic resolution imaging of the studied microstructures. Data were collected with Themis-Z using high-angle annular dark-field (HAADF) detector and low CL (73 mm) to emphasize Z-contrast of the phases. **Chemical compositions of the latter were analyzed from data collected by Super-X energy dispersive X-ray spectroscopy (EDS) detector in Themis-Z**. The data were collected and processed using the TFS Velox software. In particular, the raw data in the original spectral maps were quantified using standard Cliff-Lorimer (K-factor) fit, including absorption correction and background subtraction. Quantification was carried out considering the deconvolution of C, O, Cu and using Kα-spectral lines for Al, Ti, Nb, V, Zr, and Lα-lines for Ta. The atomic resolution and STEM-DCI images were corrected for possible sample drift and scanning beam distortions using the drift corrected frame integration (DCFI) function of Velox.

- **Details of accomplishments. Significant results [6]**

Alloy in condition 2 (As Cast + 1200°C / 24 h + 1200°C / 2h WQ) strained at 600°C

The key outcomes of the microstructure investigation of $Al_{0.5}NbTa_{0.8}Ti_{1.5}V_{0.2}Zr$ in condition 2 could be listed as follows:

1. The initial solutionized microstructure is highly metastable. Whereas nano-clusters of B2 phase are initially embedded in the BCC matrix after solutionizing, the ordered phase appears larger and aligned along <100> directions after mechanical testing at 10^{-4} s^{-1}. B2 precipitates are Al/Zr enriched and Nb/Ta depleted.
2. Deformation occurs by a/2<111> weakly paired dislocations which often appear along

the screw component. Dislocations are observed as highly pinned on B2 precipitates and should shear the latter in a cooperative process.

3. Dislocations are confined in bands, which are not – on average – parallel to a low-index crystallographic planes but lie in-between {110} and {112} highlighting intense cross-slip processes at 600°C.
4. STEM observations bring to light that plasticity is remarkably constrained in narrow regions due the presence of the B2 phase. Bands mainly consist of facets along {110} but some parallel to {112} appear.
5. A significant segregation effect is observed in the deformation bands with a Ti enrichment and a Nb/Ta depletion. Even if the effect needs additional work, it seems reasonable to associate such phenomenon with a potential decrease of the APB energy, as observed in other metallic systems.

The overview of the initial microstructure after annealing at 1200°C / 2h followed by WQ and prior mechanical testing is given in Fig. 1. HAADF-STEM image obtained in [001] zone axis condition in Fig. 1a shows that the atomic structure of the alloy mainly represents a BCC crystal structure along with the presence of an additional long-range ordered phase. The latter is evidenced by the existence of low-intensity diffraction extra superlattice spots at half distance of the {200} BCC spots in the fast Fourier transform (FFT) and which correspond to the B2 structure (inset of Fig. 1a). Precipitates appear as nano-clusters embedded in the BCC matrix phase, and are homogenously distributed in the BCC matrix with some clusters elongated along the <001> directions as observed in Fig. 1b after filtering the image using only the superlattice B2 reflections. Fig. 1c shows STEM-EDS mapping of elements distribution in the initial microstructure. No clear elemental segregation is observed but some slight increase of Al and Zr content could be associated with the presence of a B2 cluster (inset on Fig. 1c) probed in the center of the profile (Fig. 1d).

The microstructure features after the compression test at 600°C with strain rate of 10^{-4} s^{-1} the (yield stress and true stress after 0.040 true strain were 1186 MPa and 1457 MPa, respectively) and subsequent FIB extraction of a TEM foil along a <001> direction are shown in Fig. 2. HAADF-STEM image (Fig. 2a) shows a microstructure, which has significantly evolved with respect to the initial state (compare Fig. 2a to Fig. 1). In that respect, Fig. 2 reveals the presence of two phases with distinct Z-contrast. The dark regions of the microstructure correspond to a phase with the ordered B2 crystal structure, which is confirmed by the presence of {001} superlattice reflections (see the FFT diffraction pattern in inset of Fig. 2a), and the difference in HAADF intensity of atomic columns along the [110] direction (Fig. 2b). While the column intensities are roughly identical in the BCC phase, differences are noticeable in the B2 areas, corresponding to chemical changes between the two lattice sites of the ordered structure (Fig. 2d). The B2 precipitates are elongated along <100> directions of the BCC matrix, their average width is less than 2 nm and their length is ranging from about 10 to 30 nm (Figs. 2b and 2c). The BCC/B2 interfaces are wavy with possible presence of steps, but appear also diffuse due to some compositional gradient between the two phases. Finally, it is worth noting that the cube-to-cube coherency between the two phases is maintained as it is clearly evidenced from observed

<100>B2 || <100>BCC and {110}B2 || {110}BCC orientation relationships (Figs. 2b and 2c).

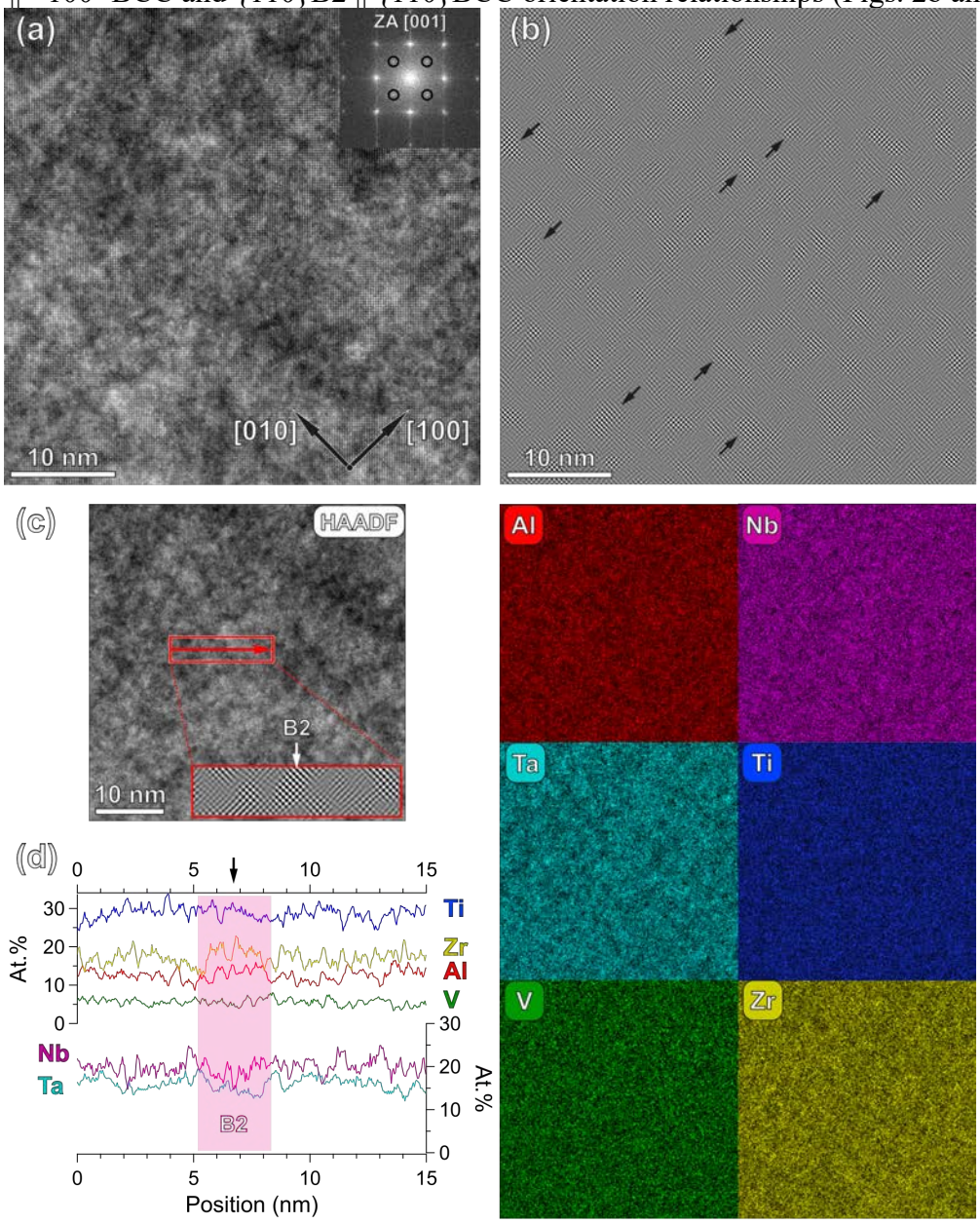

Figure 1. HAADF-STEM micrographs of the initial microstructure of Al0.5NbTa0.8Ti1.5V0.2Zr in the annealed condition (1200°C for 2 h + WQ, see section 2). (a) Unfiltered micrograph showing the atomic structure in the [001] zone axis. The inset shows the FFT diffraction pattern which reveals the presence of {001} superlattice reflections of the B2 phase. (b) Corresponding image after FFT filtering using only {001} B2 reflections. Black arrows indicate examples of B2 clusters in the BCC matrix. (c) STEM-EDS maps of the microstructure. The inset corresponds to the magnification (inverse FFT with masks on {001} B2 superlattice reflections) of the region analyzed in (d). The white arrow points out the presence of a B2 cluster. (d) Elemental line profile analysis (red box in (c)). The vertical arrow indicates the position for which Al and Zr content slightly increase. The profile length is 15 nm, the width integration is 3.5 nm.

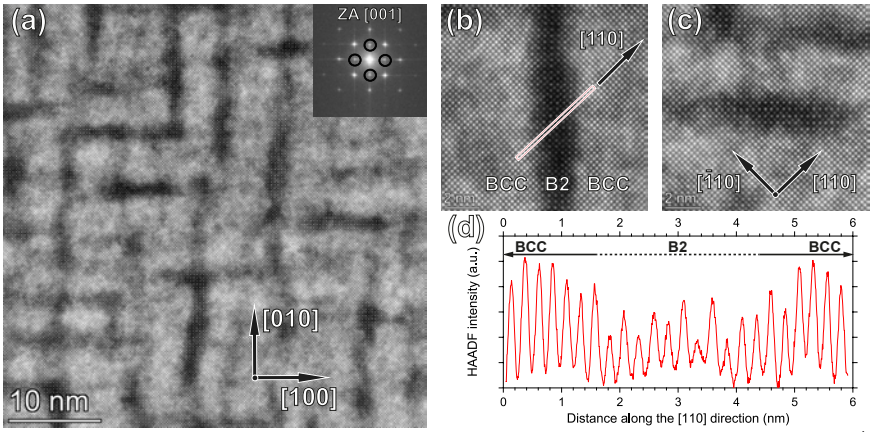

Figure 2. HAADF-STEM micrographs of the alloy microstructure after deformation at 600°C, 10^{-4} s^{-1} (plastic deformation εp~0.03). (a) Overview. FFT diffraction pattern revealing presence of {001} superlattice reflections is shown in the inset. (b), (c) Details of the B2 phase. (d) HAADF-STEM intensity of atomic columns plotted along the [110] direction as marked in (b). Background was subtracted from the HAADF-STEM signal using a polynomial law (5th order).

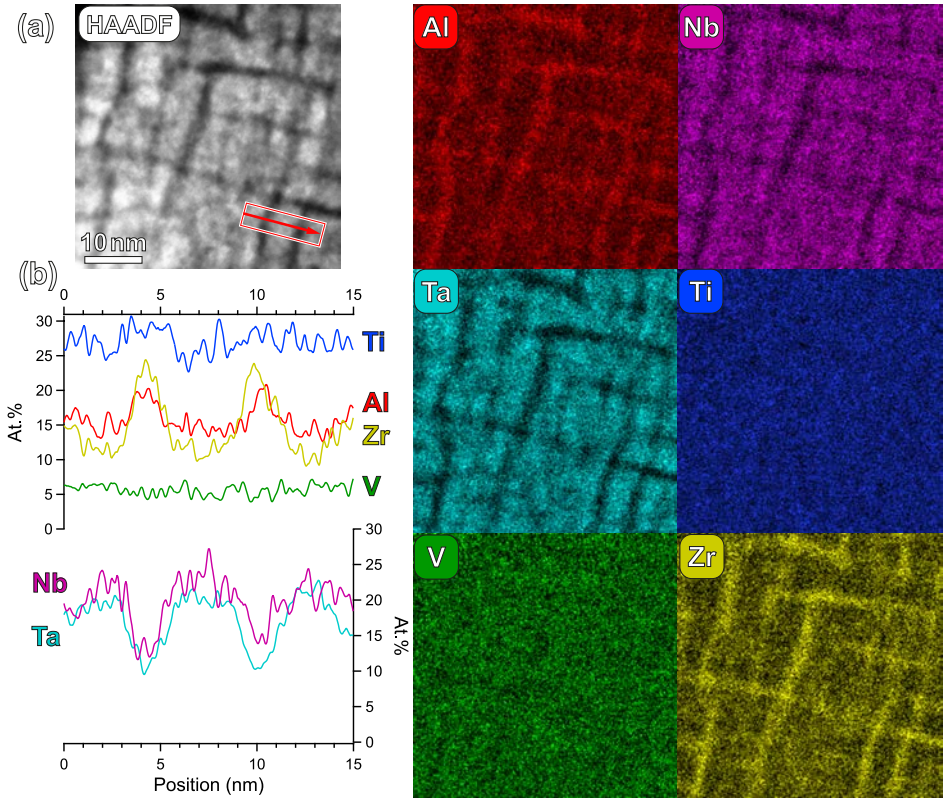

Figure 3. (a) STEM-EDS elemental maps of the two-phase nanostructure observed after compressive testing at 600°C. (b) Elemental line profile analysis corresponding to the red box in (a). The length of the line scan is 15 nm, and width integration was performed over 4.5 nm.

The presence of the two-phase microstructure is also associated with elemental partition as shown in Fig. 3. Elemental mappings using STEM-EDS highlight the depletion of Nb and Ta and the associated enrichment of Al and Zr in B2 regions (Fig. 3a). The trend is confirmed with the elemental line profile in Fig. 3b (orientation of the line profile scan is depicted in Fig. 3a) which provides the evidence that the B2 precipitation is an (Al,Zr)-rich phase. No clear tendency is observed for Ti and V partitioning as both elements appear to be homogeneously distributed in the two phases.

The analysis of the dislocation substructure after compressive testing at 600°C has been conducted on several samples with different crystallographic orientations by STEM. Some detailed STEM observations are shown in Fig. 4 for a grain strained along [251]. In that condition, the highest SF of 0.49 is found for [-1-11](011). Along the [-1-11] slip direction, Schmid factors (SFs) for [-1-11](1-2-1) and [-1-11](112) reach the same value of 0.42. Two slip traces were observed by SEM at the sample surface (not shown in the current report) and a TEM foil was extracted roughly parallel to the expected [-1-11](011) system with the highest SF. BF-STEM details the observations performed in the tilted foil with the electron beam parallel to [011] (Fig. 4). Low magnification images taken under two-beam conditions (Fig. 4a) and zone axis BF-STEM (Fig. 4b) diffraction contrast imaging conditions show two active systems – S1 and S2 (S2 is very inclined in the foil, *i.e.* the apparent thickness is small) – and a heterogenous deformation microstructure with "hard" zones made of high dislocation density bands separated by "soft" free-dislocation areas. Higher magnification reveals the dislocation content in the different sample regions (Fig. 4c). In the top and bottom parts of Fig. 4c, formation of bands appears incomplete with a variable dislocation density. In those regions, observations emphasize that most of the defects consist of widely spaced pairs of dislocations parallel to the [11-1] direction, but a few segments aligned in non-screw orientation are also pointed out. Dislocations along [11-1] are not perfectly straight as screw dislocations in BCC metals and (dilute) alloys in the low temperature regime, but rather are clearly wavy around the mean [11-1] direction (Figs. 4b and 4c). An example is given at high magnification in Fig. 4c. The two imaged dislocations appear generally parallel to each other, but are heavily pinned all along their lines by localized obstacles, presumably related to the presence of the nanoscale, ordered B2 region.

The dislocation and trace analyses confirm the presence of two slip systems, S1 and S2. Analysis of the S1-S2 systems and the use of invisibility condition is consistent with dislocations with Burgers' vector b=±a/2[11-1] for S1 (see for example Fig. 4e, and invisibility of S1 with g=[2-11]) and b=±a/2[-111] for S2. Dislocations are then mostly of screw character and arranged in planes which do not exactly correspond to {110} or {112} planes. The composite glide is emphasized in closely spaced bands in the middle of the Fig. 4c which lie between (112) (SF=0.42) and (011) (SF=0.49). This observation of composite glide coupled with the screw character of the defects confirms the presence of intense cross slip at 600°C.

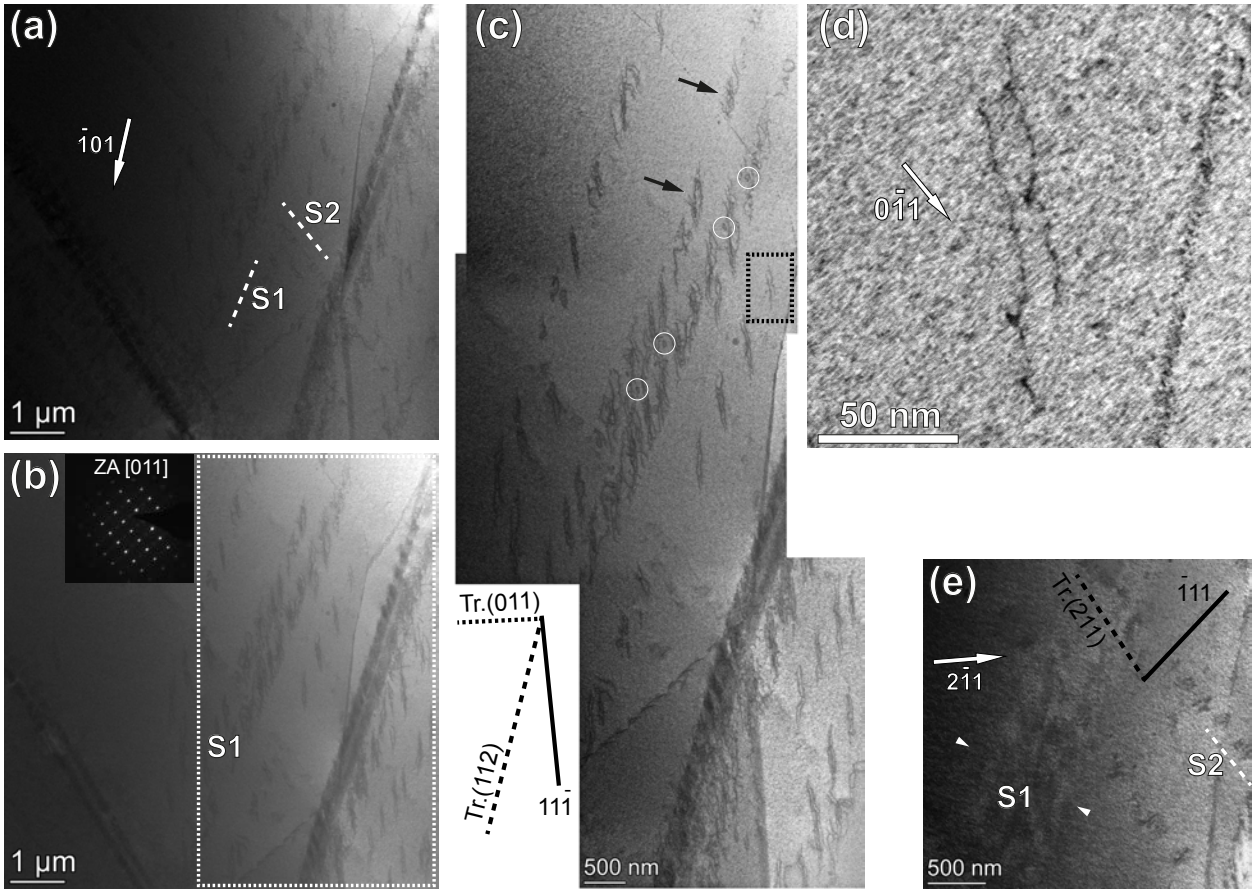

Figure 4. BF-STEM DCI images revealing the dislocation configuration in the foil extracted parallel to a deformation band. (a) Low magnification (g=[-101]) of the band structure. (b) Micrograph taken with the electron beam parallel to [011] zone axis. The inset shows corresponding diffraction pattern. Note the presence of {001} superlattice reflections of the B2 precipitates. (c) Detail of the right part of (b). Traces of (011) and (112) planes at foil surface are given in dashed lines. Projection of the Burgers vector is also drawn in solid line. Note that circles point out the presence of small loops. Arrows show the existence of bunches of screw dislocations. (d) BF-STEM DCI micrograph of a paired dislocations (g=[0-11]). (e) Micrograph taken with g=[2-11] for which dislocations in S1 are invisible (observed contrast is residual). Dislocations in S2 are visible with g=[2-11] and the band lie close to (211).

To further detail the composite glide of dislocations in the band, FIB lift-out TEM foils were prepared, with the foil surfaces perpendicular to S1, i.e. parallel to the $(-1-11)_{BCC}$ plane. In that condition, bands were imaged in an edge-on position and along the direction parallel to the Burgers vector of S1 dislocations. Fig. 5 displays selected STEM observations of the band structure. As observed by BF- (Fig. 5a) and HAADF-STEM (Fig. 5b) imaging parallel with [11-1] zone axis, two kinds of bands are evidenced. In the region of interest, four edge-on bands are seen between which dislocation activity is noticed (Fig. 5a). At low magnification, traces appear straight and finely spaced (Fig. 5b, left part) but could also appear wavy (Fig. 5b, central part). As analyzed previously, STEM micrographs confirm that traces do not coincide with low-index crystallographic planes. Fig. 5c shows a small portion of the band which mean plane is lying between the primary and the secondary slip planes, i.e. (011) and (112), and is made of poorly

defined facets as observed in Fig. 5c. An additional striking feature is the band's discrete nature.

High-resolution HAADF-STEM hence confirms that bands are highly localized as seen in Fig. 6a. The detail of atomic structure in the two regions of Fig. 6a highlights that the band thickness is of the order of 1 nm and that the mean plane could be schematically decomposed into facets with variable lengths alternating between {110} and {112} planes. The HAADF-STEM observations also reveal that the core of the band is associated with the regions of lower intensity (Fig. 6b and 6c). High-resolution STEM-EDS experiments were performed to analyze the possible local chemical fluctuations associated with the localized core of the band. To this aim, STEM-EDS elemental maps were performed around the area of interest, and one typical example is presented in Fig. 7. Fig. 7b unambiguously shows that the band is correlated to a chemical depletion of Nb and Ta and an increase of the Ti content. The integrated line profile along a direction perpendicular to the band confirms the previous trend and demonstrates that the segregation in the band is within 1-2 at.% range for the three elements (Fig. 7c). It should be noted that Al, V and Zr do not appear to segregate in the band.

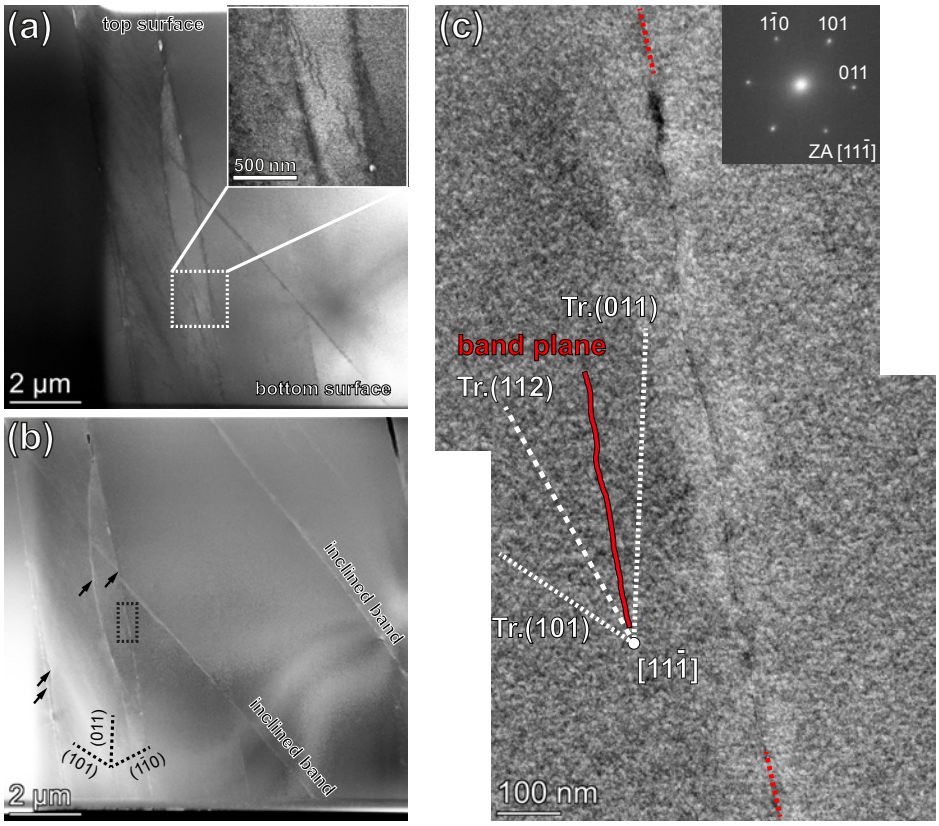

Figure 5. Microstructure imaging with the electron beam parallel to the [11-1] zone axis (a) BF-STEM diffraction contrast image (CL=360mm). (b) HAADF-STEM micrograph (CL=73mm). Arrows point out the presence of edge-on bands. Inclined bands are also observed. Dashed rectangle is imaged in detail in (c). FFT diffraction pattern is shown in the inset of (c).

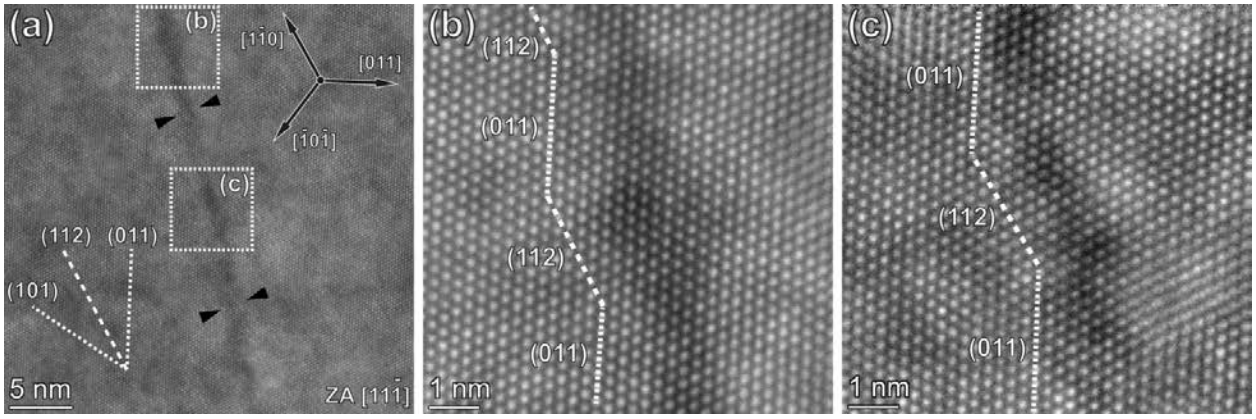

Figure 6. Atomic resolution HAADF-STEM imaging of a single band with [11-1] zone axis. (a) Overview. Black arrows point out the core of the band. <110> directions are indicated as well as (011) and (112) plane traces. Details of the atomic structure of sites marked by dashed rectangles in (a) are given in (b) and (c). Tentative of band decomposition in facets is proposed.

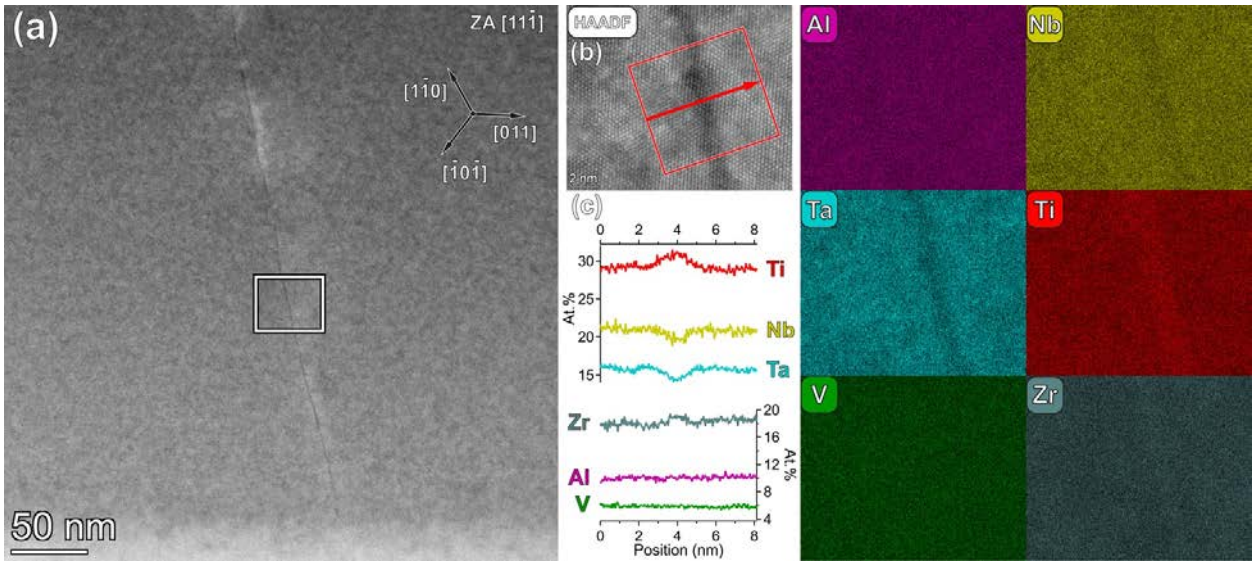

Figure 7. High spatial resolution STEM-EDS mapping of area around the band core (electron beam parallel with [11-1] zone axis) (a) HAADF-STEM overview image. The white box marks the area analyzed in (b). (b) STEM-EDS maps and corresponding HAADF-STEM Z-contrast micrograph. (c) Elemental line profile from the red area displayed in (b). The length of the line profile is 8.1 nm, and width integration was performed over 7.5 nm.

Alloy in condition 3 (As Cast + 1200°C / 24 h + 1200°C / 2h WQ + 600°C / 120h WQ) strained at 600°C

In condition 3, the long annealing at 600°C (120h) has caused the formation of discrete intermetallic phases in a disordered BCC matrix ("inverted microstructure"). After deformation at 600°C, the STEM investigation of the microstructure of the alloy in condition 3 had led to the following key outcomes (publication under preparation):

1. Apart from the disordered BCC matrix, three phases are present as discrete precipitates in the BCC matrix. They were unambiguously identified in the complex microstructure of the alloy in condition 3: the B2 phase is evidenced in high proportion and our observations bring into the light the presence of two ordered omega phases with different crystallographic structure and stoichiometry (Al_3Zr_5 and $AlZr_2$). The omega phases are derivative of the ordered B2 phase.
2. Whereas the B2 phase was coherent with the matrix in condition 2, the misfit between the two phases is estimated to 4% in condition 3. Interfacial dislocations has been evidenced between the B2 precipitates and the BCC phase.
3. Due to the large misfit between the B2 phase and the matrix, the dislocations do not shear the precipitates during the deformation at 600°C. Our observations highlight the presence of a/2<111> dislocations exclusively in the BCC matrix in which the plasticity is confined. The interesting mechanical behavior of the alloy in condition 3 is then the result of a size effect.

In condition 3, the overall microstructure of the deformed sample (600°C, εp~0.003) is given in Figure 8. STEM image is obtained along the [001] zone axis condition in the upper grain and shows the presence of discrete precipitates (dark contrast) mostly elongated along <100> direction in the matrix (grey contrast). The FFT (inset of Figure 8) confirms the existence of a B2 phase by the presence of {100} superlattice reflections. Distinct {110} and {200} reflections for both BCC and B2 phases in the FFT highlight the loss of coherency of the ordered precipitates even if the cube-to-cube orientation looks maintained. From the FFT analysis, the misfit between both phases is estimated to ~4% which leads to the existence of interfacial dislocations. The presence of such dislocations is shows in the HAADF-STEM image of Figure 9. In that case, the interface between the B2 particle and the BCC matrix is wavy (Fig. 9a) and the center of symmetry (COS) mapping technique highlights two dislocation cores (Fig. 9b). Further analysis using Nye tensor (not displayed in the current report) has revealed that the projected components of the Burgers vectors in the observation plane were a/2<110> in both cases corresponding to a/2<111> interfacial dislocations for A and B.

Our observations also evidence the presence of two additional phases derived from the B2 phase and formed during the 600°C / 120h annealing. Fig. 10 displays a high resolution HAADF-STEM in $[001]_{BCC}$ zone axis condition. The particle has facets aligned along {100} and {110} planes of the BCC phase (Fig. 10a). The analysis of the FFT allow us to confirm that the structure of the phase is $D8_8$ (ordered omega phase, hP16, Zr_5Al_3, $P6_3/mcm$) and is viewed along the [1-213] zone axis in Fig. 10b. The superposition of the atomic structure of the ordered omega with the experimental observation is perfect and confirms the $D8_8$ phase (Fig. 10c). The omega phase forms from the B2 with the collapse of pairs of {222} planes. An ordered array of vacancies is required to meet the Zr_5Al_3 stoichiometric requirement.

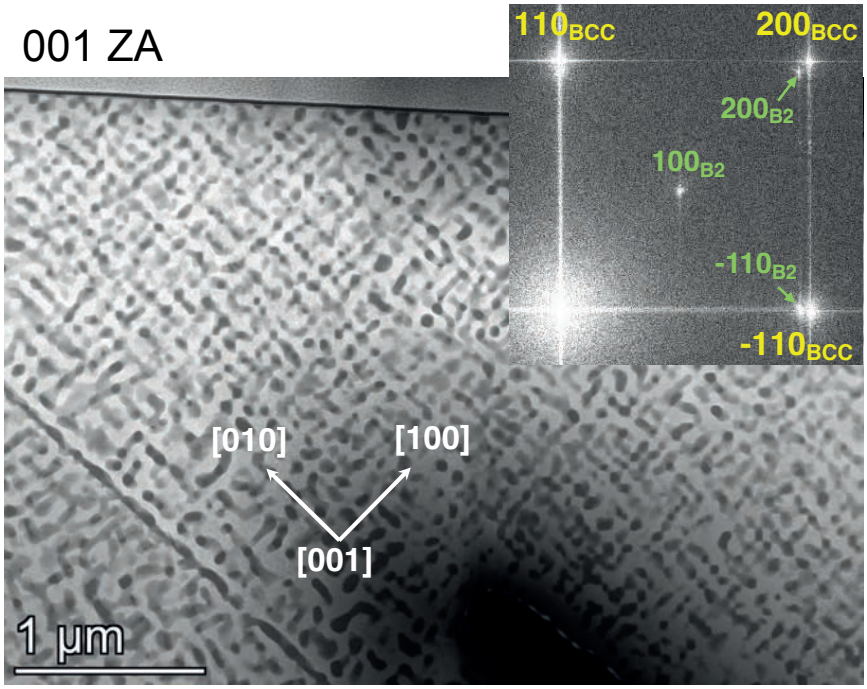

Figure 8. Microstructure imaging of the alloy in condition 3 after plastic deformation at 600°C ([001] zone axis). The inset shows the FFT of the grain in [001] zone axis. Note the presence of the B2 reflections which do not coincide with those of the BCC matrix.

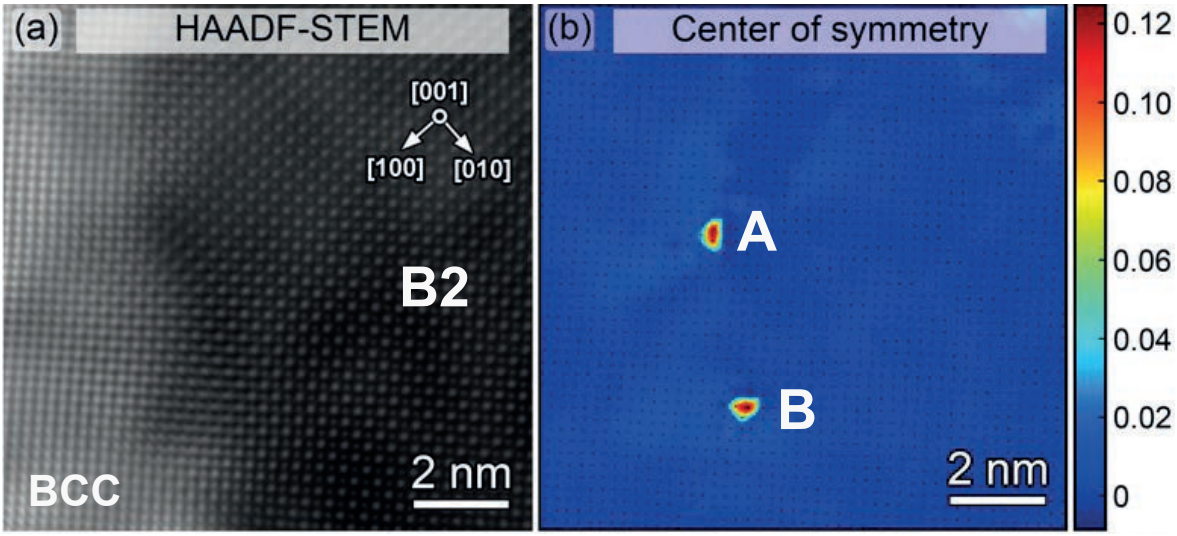

Figure 9. (a) HAADF-STEM image showing the interface between a B2 precipitate (right) and the BCC matrix (left). (b) Center of symmetry analysis highlighting the existence of 2 dislocation cores (A and B).

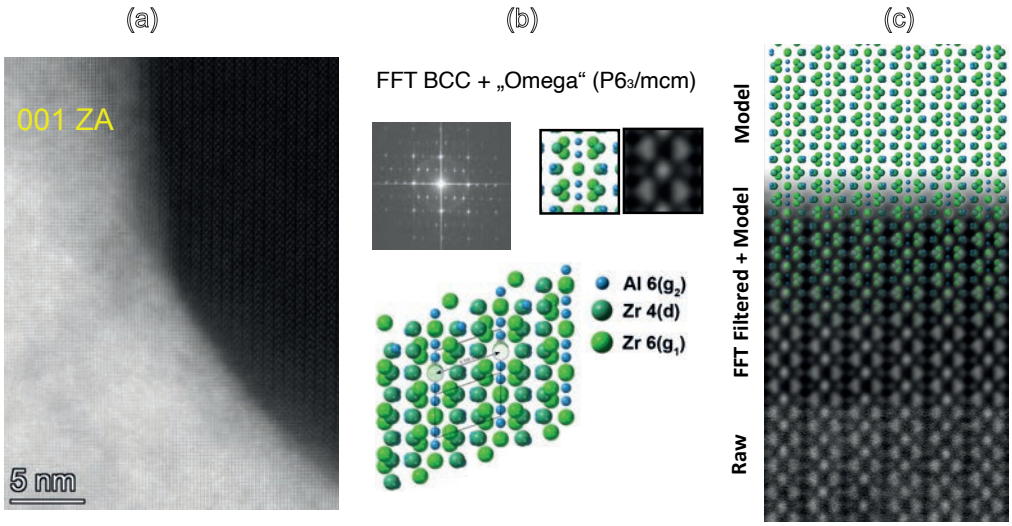

Figure 10. (a) HAADF-STEM image showing the atomic structure of the $D8_8$ omega phase (right) and the BCC matrix (left) ([001] zone axis). (b) Experiment FFT and model used for the $D8_8$ omega phase (Wyckoff positions Al 6(g_2) = 0.60 0 0.25; Zr 4(d) = 0.33 0.66 0; Zr 6(g_1) = 0.23 0 0.25; vacancy in 0 0 0 [7]). (c) Correspondence between experimental observation and atomic model of the $D8_8$ omega phase.

A second phase is also evidenced in Figure 11 and appears as pockets in the B2 phase (Fig. 11a). In Fig. 11b, the atomic structure displays a zig-zag motif which corresponds to the $B8_2$ structure of the Zr_2Al phase (ordered omega phase, hP6, $P6_3/mmc$ [7]) along the [2-1-10] direction [8]. The zig-zag structure is perfectly reproduced using a model of an atomic structure of the Zr_2Al phase. As for the $D8_8$ phase, the $B8_2$ forms from B2 and requires the collapse of {111} planes and also a chemical ordering.

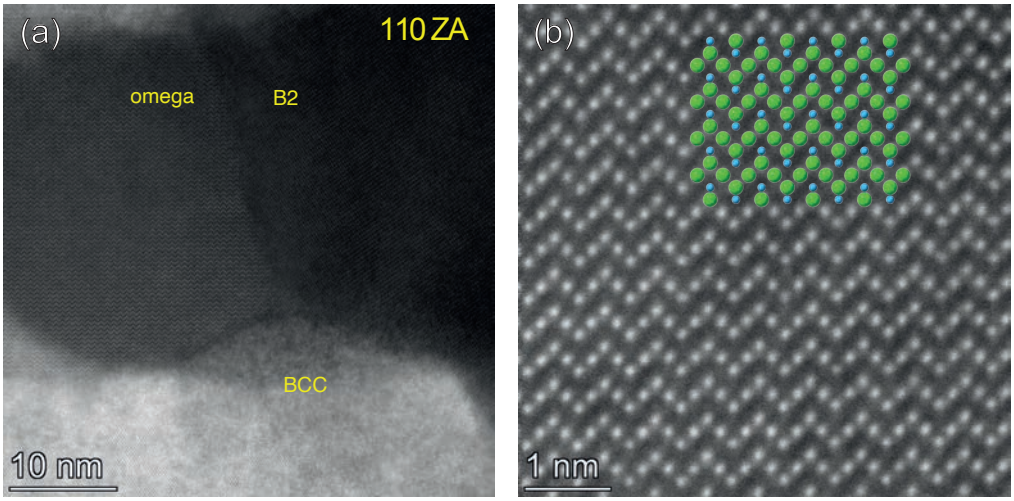

Figure 11. (a) HAADF-STEM image showing the atomic structure of the omega phase (right) and the BCC matrix (left) ([110] zone axis). (c) Correspondence between experimental observation and atomic model of the $B8_2$ omega phase. The Wyckoff positions for the $B8_2$ omega phase are: Al 2(c) = 0.33 0.66 0.25; Zr 2(d) = 0.33 0.66 0.75; 0.5Zr+0.5Al 2(a) = 0 0 0 [8].

Finally, our STEM observations reveal that the deformation is homogeneous in the sample strained at 600°C. The Burgers vector of the dislocations are of a/2<111> nature (Fig. 12a) and do not have specific orientation. Defects are observed exclusively in the disordered BCC phase and are pinned between ordered B2 or omega phases (Fig. 12b). No shearing processes of the B2 precipitates by dislocations have been evidenced which makes sense taking into account the large misfit between the B2 and the BCC phases.

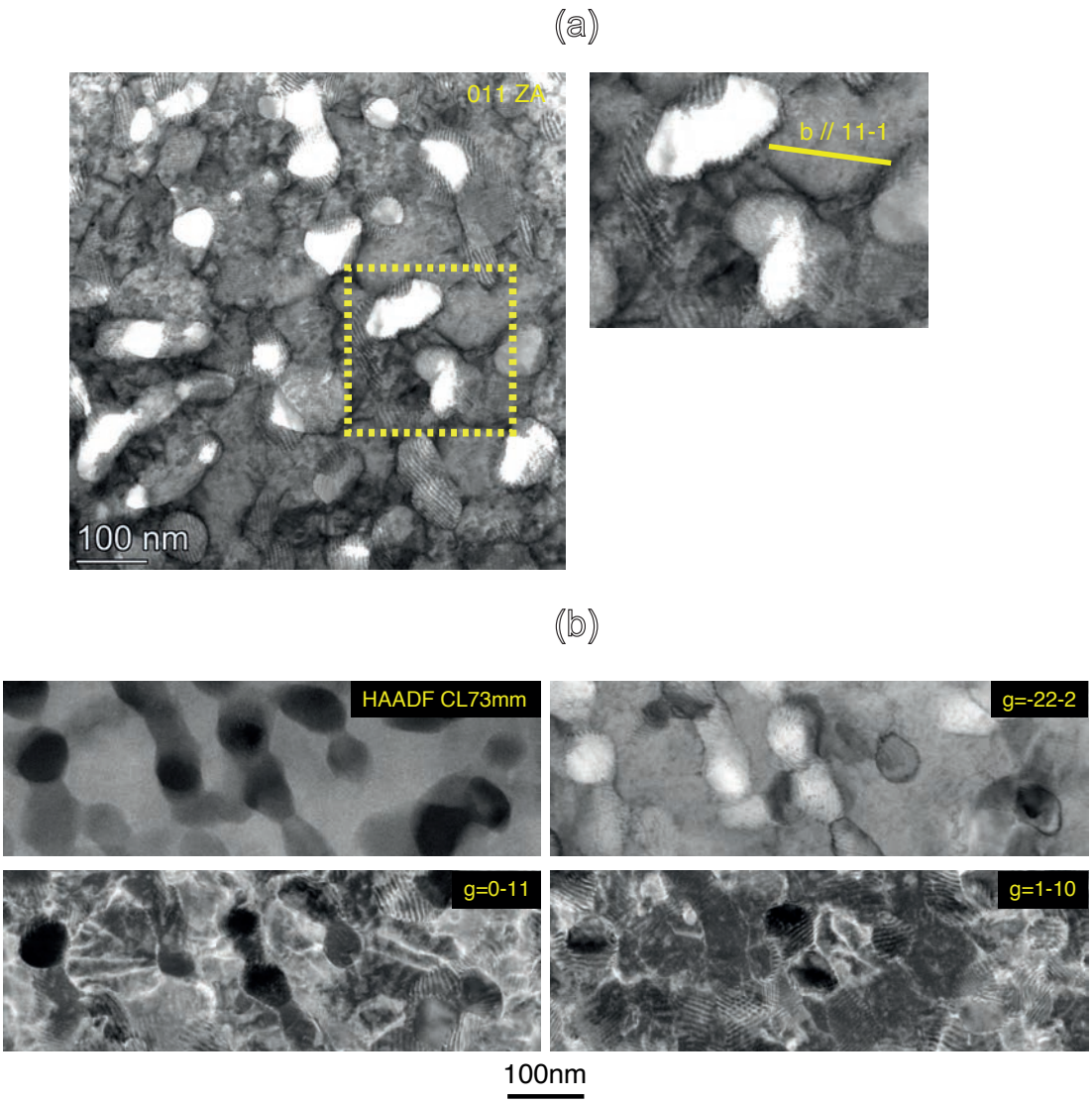

Figure 12. BF-STEM DCI images revealing the dislocation configuration in the sample in condition 3 deformed at 600°C. (a) Micrograph taken with the electron beam parallel to [011] zone axis. Note the dislocations in the BCC phase (grey contrast). Zoom of a dislocation pinned into two B2 particles sis showed in the inset. (b) Micrographs taken with different camera lengths revealing that deformation processes are constrained in the BCC phase.

References

[1] O.N. Senkov, D.B. Miracle, K.J. Chaput, J.-P. Couzinie, Development and Exploration of Refractory High Entropy Alloys – A Review, Journal of Materials Research. 33 (2018) 3092–3128. https://doi.org/10.1557/jmr.2018.153.

[2] D.B. Miracle, M.-H. Tsai, O.N. Senkov, V. Soni, R. Banerjee, Refractory high entropy superalloys (RSAs), Scripta Materialia. 187 (2020) 445–452. https://doi.org/10.1016/j.scriptamat.2020.06.048.

[3] O.N. Senkov, C. Woodward, D.B. Miracle, Microstructure and Properties of Aluminum-Containing Refractory High-Entropy Alloys, Jom. 66 (2014) 2030–2042. https://doi.org/10.1007/s11837-014-1066-0.

[4] V. Soni, O.N. Senkov, B. Gwalani, D.B. Miracle, R. Banerjee, Microstructural Design for Improving Ductility of An Initially Brittle Refractory High Entropy Alloy, Scientific Reports. 8 (2018) 8816. https://doi.org/10.1038/s41598-018-27144-3.

[5] V. Soni, B. Gwalani, T. Alam, S. Dasari, Y. Zheng, O.N. Senkov, D. Miracle, R. Banerjee, Phase inversion in a two-phase, BCC+B2, refractory high entropy alloy, Acta Materialia. 185 (2020) 89–97. https://doi.org/10.1016/j.actamat.2019.12.004.

[6] J.-P. Couzinié, M. Heczko, V. Mazánová, O.N. Senkov, M. Ghazisaeidi, R. Banerjee, M.J. Mills, High-temperature deformation mechanisms in a BCC+B2 refractory complex concentrated alloy, Acta Materialia. 233 (2022) 117995. https://doi.org/10.1016/j.actamat.2022.117995.

[7] S. Banerjee, P. Mukhopadhyay, Phase Transformations: Examples from Titanium and Zirconium Alloys, Elsevier, 2007.

[8] L.A. Bendersky, W.J. Boettinger, B.P. Burton, F.S. Biancaniello, C.B. Shoemaker, The formation of ordered ω-related phases in alloys of composition Ti4Al3Nb, Acta Metallurgica et Materialia. 38 (1990) 931–943. https://doi.org/10.1016/0956-7151(90)90165-D.

- **Dissemination of the results**

The results obtained in the framework of the project have been valued through the publications of two articles in high-impact journals:

1. Zachary T. Kloenne, Kamalnath Kadirvel, Jean-Philippe Couzinié, Gopal B. Viswanathan, Yunzhi Wang, and Hamish L. Fraser, High temperature phase stability of the compositionally complex alloy $AlMo_{0.5}NbTa_{0.5}TiZr$, Appl. Phys. Lett., 119, 151903 (2021); https://doi.org/10.1063/5.0069497

2. Jean-Philippe Couzinié, Milan Heczko, Veronika Mazánová, Oleg N. Senkov, Maryam Ghazisaeidi, Rajarshi Banerjee, Michael J.Mills, High-temperature deformation mechanisms in a BCC+B2 refractory complex concentrated alloy, Acta Materialia, 233, 117995 (2022); https://doi.org/10.1016/j.actamat.2022.117995

Results were also disseminated in conferences listed below (presenter is in **bold**):

1. CEMAS Webinar (Beyond the Scope) – June 21 2021, CEMAS-OSU, Columbus (USA)

Jean-Philippe Couzinié, Milan Heczko, Veronika Mazánová, Ashton Egal, Maryam Ghazisaeidi, Michael Mills, "*STEM, Diffraction Contrast and Defects in High Entropy Alloys Exhibiting B2-order*" (oral presentation)

2. MS&T21: Materials Science and Technology Symposium: High Entropy Materials: Concentrated Solid Solutions, Intermetallics, Ceramics, Functional Materials and Beyond II – October 17-20, 2021, Columbus (USA)

Jean-Philippe Couzinié, Milan Heczko, Veronika Mazánová, Maryam Ghazisaeidi, Oleg N. Senkov, Rajarshi Banerjee, **Michael Mills**, "Insights into the Deformation Processes of a Refractory Complex Concentrated Alloy Exhibiting B2-type Order" (invited presentation)

3. Symposium on Possibilities and Limitations of Quantitative Materials Modeling and Characterization 2021 – October 12-15, 2021, Bernkastel (Germany)

Jean-Philippe Couzinié, Clémence Tafani, Loïc Perrière, Ivan Guillot, Frederic Mompiou, Guillaume Laplanche, Tong Li, Christian Reinhart, Milan Heczko, Veronika Mazánová, Maryam Ghazisaeidi, Oleg Senkov, Dan Miracle, Rajarshi Banerjee, Michael Mills, "*Plasticity of refractory complex concentrated alloys*" (invited presentation)

4. OECD/NEA High Entropy Alloys for Nuclear Applications Workshop (Virtual) – October 19-21, 2021

Jean-Philippe Couzinié, Loïc Perrière, Ivan Guillot, Frederic Mompiou, Guillaume Laplanche, Milan Heczko, Veronika Mazánová, Maryam Ghazisaeidi, Oleg Senkov, Dan Miracle, Rajarshi Banerjee, Michael Mills, "*Mechanical properties and underlying deformation mechanisms of complex concentrated alloys: a review*" (invited presentation)

5. 2021 MRS-T international Conference – November 13-17, 2021, Taipei (Taiwan)
Jean-Philippe Couzinié, Milan Heczko, Veronika Mazánová, Zachary Kloenne, Gopal B. Viswanathan, Brian Welk, Maryam Ghazisaeidi, Hamish L. Fraser, Oleg N. Senkov, Rajarshi Banerjee, Michael Mills, "*Microstructures and deformation mechanisms of refractory complex concentrated alloys exhibiting B2 order*" (invited presentation - virtual)

6. Meeting of the GDR 2048 on Métallurgie des Alliages à Haute entropie (HEA) ou à Composition Complexe (CCA) – November 15-17, 2021, Thiais (France)
Jean-Philippe Couzinié, Milan Heczko, Veronika Mazánová, Zachary Kloenne, Gopal B. Viswanathan, Brian Welk, Maryam Ghazisaeidi, Oleg Senkov, Rajarshi Banerjee, Hamish L. Fraser, Michael Mills "*Properties of refractory complex concentrated alloys exhibiting B2 order*" (invited presentation)

7. TMS HEA2021 – December 05-08, 2021, Charlotte (USA)
Jean-Philippe Couzinié, **Milan Heczko**, Veronika Mazánová, Maryam Ghazisaeidi, Oleg N. Senkov, Rajarshi Banerjee, Michael Mills, "*Microstructure and deformation processes of a refractory complex concentrated alloy exhibiting B2-type order*" (oral presentation)

8. TMS Annual Meeting – February 27-March 03, 2022, Anaheim (USA)
Jean-Philippe Couzinié, Milan Heczko, Veronika Mazánová, Maryam Ghazisaeidi, Oleg N. Senkov, Rajarshi Banerjee, Michael Mills, "*TEM study of a refractory complex concentrated alloy with BCC/B2 microstructure*" (invited presentation)

9. TMS Annual Meeting – February 27-March 03, 2022, Anaheim (USA)
Gopal B. Viswanathan, Jean-Philippe Couzinié, Zachary Kloenne, Brian Welk, Oleg Senkov, Hamish Fraser, "*Evolution of Microstructure and Deformation Substructure in Al1Mo0.5 Nb1Ta0.5Ti1Zr1, a Refractory HEA Alloy with Disordered BCC Precipitates Embedded in a Continuous Ordered B2 Matrix*" (invited presentation)

10. RUB-Symposium on High-, Medium-Entropy Alloys (HEAs/MEAs) and Compositionally Complex Alloys (CCAs) – March 09-10, 2022, Bochum (Germany)
Jean-Philippe Couzinié, Clémence Tafani, Thomas Rieger, Loïc Perrière, Jean-Marc Joubert, Frederic Mompiou, Daniel Caillard, Christian Wagner, Guillaume Laplanche, Milan Heczko, Veronika Mazánová, Maryam Ghazisaeidi, Oleg Senkov, Rajarshi Banerjee, Michael Mills, "*CC alloys strengthened by ordered phases: Design, microstructures and deformation mechanisms*" (invited presentation)

11. French symposium on Plasticity (Plasticité 2020) – April 04-06, 2022, Toulouse (France)
Jean-Philippe Couzinié, Loïc Perrière, Frederic Mompiou, Daniel Caillard, Christian Wagner, Guillaume Laplanche, Milan Heczko, Veronika Mazánová, Maryam Ghazisaeidi, Oleg Senkov, Rajarshi Banerjee, Michael Mills, "*Plasticité d'alliages réfractaires de composition complexe et de structure cubique centrée*" (invited presentation)

12. International Conference on Strength of Materials (ICSMA 19th) – June 26-July 01, 2022, Metz (France)

Jean-Philippe Couzinié, Clémence Tafani, Frederic Mompiou, Daniel Caillard, Christian Wagner, Guillaume Laplanche, Milan Heczko, Veronika Mazánová, Maryam Ghazisaeidi, Oleg Senkov, Rajarshi Banerjee, Michael Mills "*Deformation processes of refractory complex alloys with BCC/B2 microstructure*" (plenary conference)

Impacts

Development of the principal discipline(s) of the project

Slip transmission between bcc/B2 regions with various degrees of order are lacking in the literature, but it is crucial to understand these behaviors with respect to the emerging BCC/B2 alloy systems. Slip transmission is an incredibly "rich" field even in superalloys, where a relatively simple OR between FCC matrix and precipitates exists. Similarly, this work has demonstrated that slip transmission in the BCC/B2 microstructures may hold the key to understanding material strength retention at higher temperatures. The present work is the first comprehensive study of slip transmission and deformation mechanisms in BCC/B2 alloy systems has yet to be conducted.

Development of the principal discipline(s) of the project

This work was disseminated in a high-profile publication in Acta Materialia, and was also presented at numerous high-profile meetings and conferences. The local compositional fluctuations that we have detected at slip bands after high temperature deformation are likely to be a common phenomenon in refractory high entropy alloys. This effect has not been considered previously in any previous models for behavior of these alloys, and will spawn DFT and continuum model development.

Other disciplines

Development of viable refractory alloys for ultra-high temperature applications have important implications for materials applications under extreme conditions, including aerospace and hypersonics. Fundamental understanding of behavior in emerging systems such as alloys with the BCC/B2 microstructure will help guide future alloy development efforts.

Describe the impact in this reporting period on the development of human resources

This work involved extensive interaction between Profs. Couzinié and Mills with a senior undergraduate, Bryan Crossman, who is now a graduate student in the MSE Department at OSU. This work also involved extensive collaboration with post-doctoral associates Milan Heczko and Veronika Mazánová, who learned techniques related to defect analysis in BCC microstructures from Prof. Couzinié.

Describe the impact on teaching and educational experiences

The sophisticated, multi-scale characterization approach used in this work is a model for the analysis of complex deformation behavior. This streamlined workflow developed in this work will be incorporated into graduate level characterization classes at OSU and its affiliate institutions (e.g. University of Dayton and Case Western Reserve University).

Describe the impact in this reporting period on physical, institutional, and information resources that form infrastructure

Nothing to report.

Impact on society beyond science and technology

Nothing to report.

Changes

Nothing to report.

Technical Updates

Nothing to report.


AIR FORCE OFFICE OF SCIENTIFIC RESEARCH
UNITED STATES AIR FORCE